Acta Crystallographica Section D
Biological Crystallography
ISSN 0907-4449

Crystallization by capillary counter-diffusion and structure determination of the N114A mutant of the SH3 domain of Abl tyrosine kinase complexed with a high-affinity peptide ligand

Ana Cámara-Artigas,[a] Andrés Palencia,[b] José C. Martínez,[b] Irene Luque,[b] José Antonio Gavira[c] and Juan Manuel García-Ruiz[c]*

[a]Departamento de Química Física, Bioquímica y Química Inorgánica, Universidad de Almería, 04120 Almería, Spain, [b]Departamento de Química Física e Instituto de Biotecnología, Facultad de Ciencias, Universidad de Granada, 18071 Granada, Spain, and [c]Laboratorio de Estudios Cristalográficos, P. T. Ciencias de la Salud, Edf. BIC-Granada, 18100 Armilla, Granada, Spain

Correspondence e-mail: jmgruiz@ugr.es

Received 16 December 2006
Accepted 9 March 2007

PDB Reference: N114A Abl-SH32–p41 complex, 2o88, r2o88sf.

The recognition of proline-rich ligands by SH3 domains is part of the process leading to diseases such as cancer or AIDS. Understanding the molecular determinants of the binding affinity and specificity of these interactions is crucial for the development of potent inhibitors with therapeutic potential. In this study, the crystallographic structure of the N114A mutant of the SH3 domain of the Abelson leukaemia virus tyrosine kinase complexed with a high-affinity peptide is presented. The crystallization was carried out using the capillary counter-diffusion technique, which facilitates the screening, manipulation and transport of the crystals and allows the collection of X-ray data directly from the capillary in which the crystals were grown. The crystals of the N114A mutant belong to the orthorhombic $P2_12_12_1$ space group, with unit-cell parameters $a = 48.2$, $b = 50.1$, $c = 56.4$ Å. The quality of the diffraction data set has allowed the structure of the complex to be determined at a resolution limit of 1.75 Å.

1. Introduction

Nonreceptor tyrosine kinases catalyze the phosphorylation of a tyrosine residue in their target proteins and play an important role in the intracellular signal transduction networks that regulate the cell cycle. Tyrosine kinases contain an Src homology 3 (SH3) domain that is responsible for the recruitment of substrates and the regulation of kinase activity *via* the establishment of transient interactions with proline-rich sequences in their partners. Disruption of these regulation elements frequently leads to oncogenicity and disease. This is the case in the Abl (Abelson leukaemia virus) tyrosine kinase, which becomes constitutively activated upon deletion or mutation of its SH3 domain, causing chronic myelogenous leukaemia. The importance of SH3 interactions is further underlined by the fact that the displacement of the SH3 domain by high-affinity ligands has been shown to enhance the inhibitory effect of the antitumour drug Gleevec (Barila & Superti-Furga, 1998).

The development of small molecules that could interfere selectively with these interactions has emerged as a novel strategy for the identification of new therapeutic agents. The low affinity and selectivity of SH3 domains for their natural ligands, along with the poor understanding of the molecular determinants of binding affinity and specificity, have made the development of high-affinity ligands particularly challenging. Additionally, recent thermodynamic and structural studies (Pisabarro *et al.*, 1998; Palencia *et al.*, 2004) have revealed an unexpected complexity of these interactions; several factors, such as the presence of water molecules at the binding interfaces and the conformational equilibrium of both the protein

and the ligand, have been identified as contributing significantly to the binding energetics. These results underline the importance of the structural analysis of any possible conformational changes upon complexation and particularly of the elucidation of the presence of water molecules at the binding interface. In this manuscript, we present the crystallographic structure of a complex between the high-affinity ligand p41 and the mutant N114A of Abl-SH3, in which the side chain of Asn114 that participates in water interactions in the WT complex has been eliminated.

Because of their small size (6.9 kDa), SH3 domains and their complexes are amenable to structure determination by NMR techniques. However, a clear advantage of X-ray structural approaches is the possibility of accurately modelling the solvent molecules. Crystals of good quality were obtained by the counter-diffusion technique (García-Ruiz, 2003) using small-diameter capillaries, allowing a complete X-ray diffraction data set to be obtained from crystals located in the crystallization capillary without any further manipulation.

2. Materials and methods

2.1. Mutagenesis, expression and purification of the Abl-SH3 domain and variants

The N114A mutant of the Abl-SH3 domain was constructed using the QuikChange Site-Directed Mutagenesis Kit (Stratagene) by polymerase chain reaction, using the plasmid pBAT4 (Peranen *et al.*, 1996) containing the wild-type Abl-SH3 domain (Palencia *et al.*, 2004) as a template. The required oligonucleotides were purchased from Bonsai Technologies (Madrid, Spain). All mutations were verified by DNA sequencing (Instituto de Parasitología y Biomedicina 'López-Neyra', CSIC, Granada, Spain). The N114A mutant of the Abl-SH3 domain was expressed and purified as described previously for the wild-type protein (Musacchio *et al.*, 1994; Viguera *et al.*, 1994). Briefly, the plasmid-encoded Abl-SH3 domain was expressed in *Escherichia coli* BL21 (DE3) strain (Stratagene) using IPTG as an inducing agent. Cells were resuspended in 100 m*M* Tris pH 9.0 buffer and lysed by two passes through a French pressure cell. The domain was precipitated from the supernatant using ammonium sulfate at 75% saturation and was resuspended in 10 m*M* phosphate buffer, 500 m*M* sodium chloride pH 6.5. The protein was further purified on a Superdex-75 column equilibrated and eluted with the same buffer. Fractions containing protein were pooled, concentrated and stored at 203 K at approximately 10 mg ml^{-1} in the same buffer. The N114A mutant of the Abl-SH3 domain is stable for several months under these conditions. Protein purity was checked by SDS–PAGE and mass spectrometry and was estimated to be higher than 99%.

2.2. Peptide ligand

The peptide p41 (APSYSPPPPP) was obtained from Sigma-Genosys. The peptide was acetylated and amidated at the N- and C-termini, respectively, in order to eliminate the charges at its ends that could interfere with binding and also to mimic more closely the peptide sequence in the context of the full-length protein. The peptide was synthesized in the solid phase on an MPS column and its molecular mass was confirmed by mass spectrometry. Peptide purity (95%) was assessed by analytical HPLC.

2.3. Crystallization and data collection

Crystals were obtained by capillary counter-diffusion techniques using the new Granada Crystallization Boxes (GCB-Domino) and capillaries of 0.1 mm inner diameter supplied by Triana S&T (http://www.trianatech.com). The length of the capillaries was 60 mm and they were filled with less than 350 nl protein solution. Six GCBs were used to perform a crystallization screening of ammonium sulfate *versus* pH. The GCBs were filled with 3 *M* ammonium sulfate buffered at various pH values: 0.1 *M* sodium citrate pH 3 and 4, 0.1 *M* sodium acetate pH 5, 0.1 *M* MES pH 6, 0.1 *M* HEPES pH 7, 0.1 *M* Tris–HCl pH 8 and 0.1 *M* Bicine pH 9. The precipitant solution was covered with a plug of agarose gel at a concentration of 0.5%. The purified protein, dialyzed against 50 m*M* glycine buffer pH 3.0 and at a final protein concentration of 8 mg ml^{-1}, was mixed in a molar protein:ligand ratio of 1:2 with lyophilized p41 and the capillaries were filled with the same protein–ligand solution by capillary force. One of the ends was then sealed with wax and the capillary was punched into the GCB (Fig. 1). The operation is simple and fast: using the filled GCB provided by Triana S&T, set-up of the experiment takes no more than 45 s per capillary. The crystallization experiments were stored at room temperature (293 $\pm$ 2 K).

X-ray data were collected from crystals inside the capillary in which they were grown, thus avoiding the manipulation associated with harvesting from solution and mounting (Ng *et al.*, 2003). With this aim, the best crystals for data collection needed to be identified using a binocular lens. We looked for single and isolated crystals with distances from closest neighbours that were longer than the size of the X-ray beam. Once the crystals had been identified, their locations were marked, a capillary segment of approximately 15 mm containing the selected crystal was cut out and its ends were sealed with wax. Finally, the capillary was glued to a Copper CrystalCap (Hampton Research; http://hamptonresearch.com) and centred in the beam. X-ray diffraction data were recorded on a Bruker Smart6000 CCD detector with Kappa configuration (X8 Proteum) using Cu $K\alpha$ radiation from a Bruker Microstar micro-focus (Montel Optics) rotating-anode generator operating at 45 kV and 60 mA. A total of 459 images of 1° oscillation were collected at room temperature. Integrated intensity information for each reflection was obtained, scaled with *SAINT* (Bruker AXS Inc.) and corrected for absorption with *SADABS* (Bruker AXS Inc.) from the *PROTEUM* software suite. A summary of the data-collection statistics is shown in Table 1.

2.4. Structure resolution and refinement

Initial phasing was performed using *MOLREP* (Vagin & Teplyakov, 1997), making use of the coordinates of the WT

Table 1
X-ray data-collection and refinement statistics.

Values in parentheses are for the highest resolution bin.

Data collection	
Space group	$P2_12_12_1$
Unit-cell parameters	a = 48.170, b = 50.093, c = 56.431
Resolution range (Å)	50.0–1.75 (1.85–1.75)
No. of observations	84702
Unique reflections	13236 (1638)
Data completeness (%)	92.2 (75.8)
R_{sym}† (%)	0.07 (0.24)
$\langle I/\sigma(I)\rangle$	16.4 (4.4)
Refinement	
Protein residues	57 (chain *A*), 55 (chain *B*)
Solvent molecules	69
R_{work} (%)	16.9 (20.5)
R_{free} (%)	21.5 (26.8)
R.m.s. deviations from ideal geometry	
Bonds (Å)	0.008
Angles (°)	1.740
Mean B, protein (Å^2)	24.1
Mean B, solvent (Å^2)	35.28
Residues in most favoured regions of the Ramachandran plot‡ (%)	100

† $R_{sym} = \sum_{\mathbf{h}}\sum_l |I_{\mathbf{h}l} - \langle I_{\mathbf{h}}\rangle| / \sum_{\mathbf{h}}\sum_l \langle I_{\mathbf{h}}\rangle$, where I_l is the lth observation of reflection **h** and $\langle I_{\mathbf{h}}\rangle$ is the weighted average intensity for all observations l of reflection **h**. ‡ From *PROCHECK* statistics.

Abl-SH3 domain complexed with the high-affinity ligand p41 (PDB code 1bbz; Pisabarro *et al.*, 1998), from which the peptide ligand and water molecules had been removed. The molecular-replacement solution refinement was conducted using several cycles of restrained positional and temperature-factor refinement in *REFMAC*5 from the *CCP*4 suite (Collaborative Computational Project, Number 4, 1994), alternated with manual building using the resulting σ_A-weighted $(2F_o - F_c)$ and $(F_o - F_c)$ electron-density maps in *Coot* (Emsley & Cowtan, 2004). Because two molecules of the Abl-SH3–p41 complex were found in the asymmetric unit, the refinement was conducted using noncrystallographic symmetry restraints. At the final stage of refinement, TLS parameters (Winn *et al.*, 2003) defined for each of the TLS domains using the *TLSMD* server (Painter & Merritt, 2006) were included. Water molecules were placed in the electron-density difference maps using *ARP*/*wARP* v.5.0 from the *CCP*4 suite. All the structures were checked using *PROCHECK* (Laskowski *et al.*, 1993). Structure-refinement statistics are compiled in Table 1.

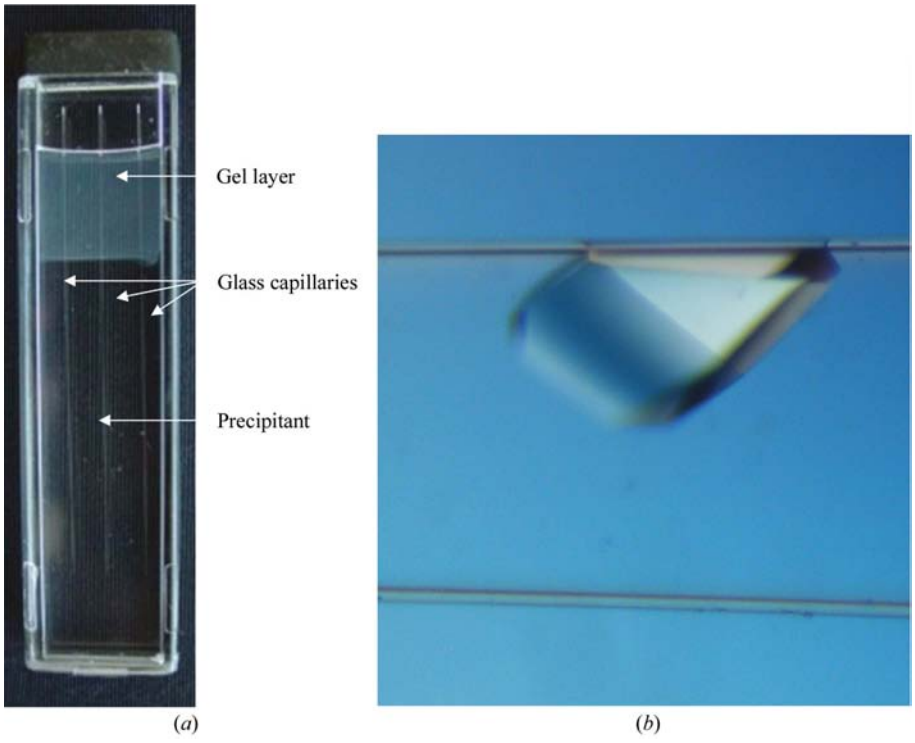

Figure 1
(*a*) A GCB-Domino box as used for the crystallization experiments (García-Ruiz & González-Ramírez, 2006). (*b*) A crystal of the N114A mutant of the SH3 domain of Ab1 complexed with the p41 decapeptide grown by the capillary counter-diffusion technique. The diameter of the capillary is 0.1 mm and its length is 60 mm. This picture was obtained 5 d after setting up the experiment.

3. Results and discussion

3.1. Crystallization of N114A mutant with the peptide ligand

The crystallization screen was performed in capillaries. Because the WT protein was crystallized with ammonium sulfate, the screening was restricted to revealing the effect of this salt on crystallization at six different pH values from 4 to 9. One of the advantages of the counter-diffusion technique is its ability to explore in one single experiment all the precipitant concentration values from the starting concentration (3 *M*). Therefore, the screening was reduced to only six capillaries. Crystals were obtained at pH values of 6, 7 and 8. The best crystals in terms of facetting, size and optical transparency were grown at pH 7 (Fig. 1). No optimization was performed; the crystals obtained in the first screening were used for X-ray diffraction. Data collection was performed directly from the capillary without additional handling. Crystals of the N114A mutant with the peptide ligand were found to grow in the orthorhombic space group $P2_12_12_1$, with unit-cell parameters a = 48.2, b = 50.1, c = 56.4 Å and a unit-cell volume of 136 167 Å^3. Two monomers can be placed in the unit cell to yield a Matthews coefficient of 2.10 Å^3 Da^{-1} and a solvent content of 41.5% (Matthews, 1968). The space-group assignment was made based upon the agreement of the intensities of symmetry-related reflections and from the systematic absences. The space group is maintained with regard to the WT Abl-SH3–p41 complex, although the unit-cell parameters of the mutant differ from those found for the WT

complex, which had unit-cell parameters a = 46.7, b = 73.8, c = 80.0 Å and a unit-cell volume of 254 863 Å^3. The placement of four monomers yielded a Matthews coefficient of 1.97 Å^3 Da^{-1}, with a solvent content of 37.5%. Packing considerations will be discussed later.

The above protein crystallization results are especially interesting because the crystal diffraction took place directly from the screening results, without further optimization or handling. Modern procedures for protein crystallization require fast screening, the use of small amounts of protein solution and minimization of the manipulation of the crystals. These requirements were achieved here with the use of the capillary counter-diffusion technique. This technique can currently be implemented using a simple and fast protocol, which permits its use not only for optimization but also for screening, as demonstrated in this paper. For instance, in our case the use of capillary counter-diffusion allowed a full screening of the crystallization space defined by a pH range from 4 to 9 and a continuous range of ammonium sulfate concentration from 0 to 3 *M*. In addition, the use of new capillaries of 75 or 100 µm in diameter allows a significant reduction of the amount of protein solution required per experiment, down to a volume range of 200–400 nl. For instance, in our case the full screening of ammonium sulfate *versus* pH was achieved with only six capillaries, each of them containing about 300 nl protein solution. Furthermore, the transparency to X-rays of these thin capillaries permits X-ray diffraction directly from crystals located in the capillaries used for crystallization, allowing checking of the composition of the grown crystals, their diffraction quality and, as demonstrated in this paper, the collection of the complete diffraction data set required for structure determination.

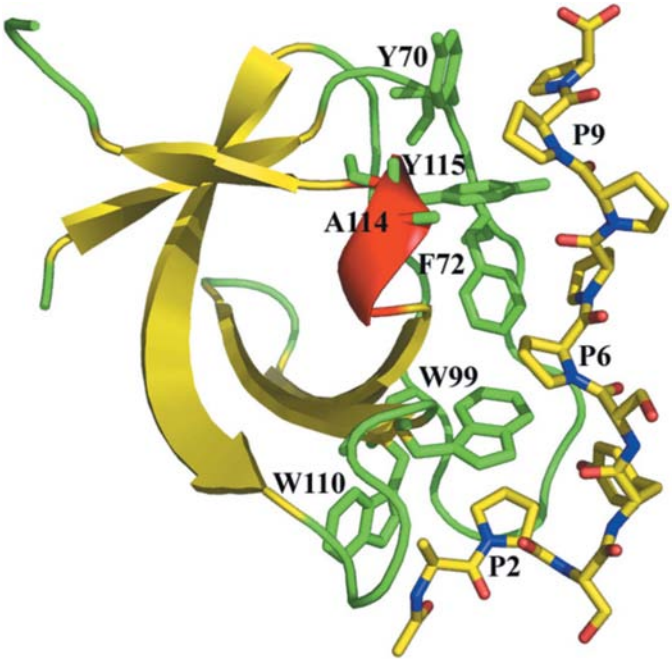

Figure 2
Overall fold of the N114A mutant of the SH3 domain of Ab1 in complex with the p41 decapeptide. Residues in the SH3 domain-binding site are shown as green sticks. The decapeptide p41 is shown as yellow sticks. The proline residues interacting with the three hydrophobic pockets (pocket 1, Tyr70/Tyr115; pocket 2, Tyr115/Phe72/Trp99; pocket 3, Trp99/Trp110/Asn78) in the SH3 domain are indicated.

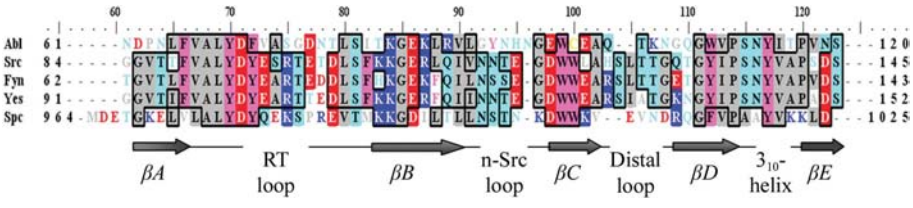

Figure 3
Sequence alignment of various SH3 domains. The corresponding secondary structures are shown at the bottom of the figure. Highly conserved residues are shown in boxes. The residues are coloured according to their nature: pink for aromatic residues, red for acidic residues, blue for basic residues, cyan for polar residues and grey for aliphatic residues.

3.2. Structure of the N114A Abl-SH3–p41 complex

A molecular-replacement search using *MOLREP* (Vagin & Teplyakov, 1997) yielded a solution with two molecules in the asymmetric unit with a correlation coefficient of 0.649, an R factor of 0.49 and contrast of 10.2. A further decrease in the R and $R_{\rm free}$ factors to values of 0.42 and 0.44, respectively, was obtained after rigid-body refinement using *REFMAC*5.0. The initial model lacked the mutated residue and peptide, but both were easily identified in an $|F_{\rm o} - F_{\rm c}|$ OMIT map and were therefore included in the model (Fig. 2). After restrained and TLS refinement using *REFMAC*5.0, the model was completed with 67 water molecules. Electron density corresponding to a sulfate anion was found next to Arg89. Refinement statistics are summarized in Table 1.

The Abl-SH3 domain is comprised of residues 61–122 of the Abl tyrosine kinase and its structure is formed by five anti-parallel β-strands arranged as two orthogonal β-sheets (Fig. 2). The overall fold of the Abl-SH3 domain is well conserved in different SH3 domains, with the main differences being found in the three loops (n-Src, RT and distal loop) that interconnect the β-strands. The high-affinity ligand p41 (APSYSPPPPP) is bound with residues 5–10 adopting a PPII helix conformation, as previously reported for the WT protein (Pisabarro *et al.*, 1998). The binding site in the SH3 domain is located in a shallow hydrophobic groove lined with highly conserved aromatic residues. Residues of the PPII region in the ligand pack closely against two hydrophobic pockets for which high sequence conservation is observed in different SH3 domains. In fact, it has been proposed that the recognition of the PPII region in the ligand is not selective. Additional interactions are established between residues flanking the P*XX*P core motif in the peptide and a third pocket, frequently called the specificity pocket, in the SH3 domains, which is delimited by the RT and n-Src loops. These loops are highly variable in sequence and have been proposed to confer specificity to the interaction (Fig. 3). A significant

level of flexibility has been reported for these loops and this has even been proposed to play an important role in molecular recognition, improving the ligand specificity by induced fit (Arold *et al.*, 1998). This is indeed the case for the SH3 domain of Abl, structures of which have been determined at high resolution over a broad range of pH values (from pH 3 to pH 8). Even in the structure with the highest resolution (1.35 Å), the high mobility of the RT loop results in a lack of corresponding electron density (Palencia *et al.*, in preparation). In contrast, the σ_A-weighted ($2F_o - F_c$) and ($F_o - F_c$) electron-density maps for the RT loop in the complexed N114A mutant described here clearly allow this loop to be modelled as a type I β-turn. As observed in other SH3 complexes, binding of the ligand results in rigidification and structural rearrangement of the RT loop in the SH3 domain.

3.3. Comparison of the N114A Abl-SH3–p41 and the WT Abl-SH3–p41 complex structures

The crystal structure of the WT Abl-SH3 domain complexed with the high-affinity synthetic decapeptide p41 has been described previously (Pisabarro *et al.*, 1998). The WT Abl-SH3–p41 crystal belongs to space group $P2_12_12_1$ and has unit-cell parameters a = 46.7, b = 73.8, c = 80.0 Å, while the unit cell of the N114A Abl-SH3–p41 complex has a much smaller volume (a = 48.2, b = 50.1, c = 56.4 Å). These differences in the unit-cell volume yield a different number of molecules in the asymmetric unit, so that for the WT structure the asymmetric unit contains four molecules of the Abl-SH3–p41 complex arranged on a pseudo-fourfold screw axis (4_1) parallel to the a axis, while only two molecules are found in the asymmetric unit of the mutant structure. Superposition of the main chains in all six complex structures (the two chains from the N114A mutant and the four chains from the WT present in the asymmetric unit) yields an average r.m.s.d. of 0.46 Å. The major differences are found in the loops, with the highest r.m.s.d. (ranging from 1.62 to 0.25 Å) found in the distal loop. Packing considerations must be taken into account in order to explain these differences. The distal loop in chain *A* of the mutant structure participates in a crystalline contact, whereas the same loop in chain *B* is solvent-exposed. In the case of the WT structure, the distal loops from chains *A* and *G* take part in a crystal contact and these of chains *C* and *E* are solvent-exposed. The same differences in r.m.s.d. are found when superposing chains *A* and *B* of the mutant complex structure and when comparing the various chains in the WT structure.

A comparison of the unit cells of the WT and mutant structures reveals that the spatial arrangements of the molecules in the two crystal forms are almost identical. In Fig. 4, chains *A* and *B* from the asymmetric unit of the mutant complex structure are compared with chains *A*, *C*, *E* and *G* from the asymmetric unit of the WT structure. The only significant difference is a 3 Å translation along the *c* axis in the superposition of chain *B* of the mutant structure with the corresponding chains *C* and *G* in the WT structure. These changes in the packing of the chains in the asymmetric unit are the result of higher symmetry in the mutant crystal, which explains the smaller unit cell needed to represent the three-dimensional arrangement of the protein complex and could be related to the higher quality of the crystal.

No significant backbone changes are associated with the mutation of Asn114 to Ala. This residue is placed at the binding site, but all the contacts with the residues of the p41 peptide are mediated by water molecules that play an important role in peptide binding, as indicated by the thermodynamic signature of the binding (Palencia *et al.*, 2004). The good quality of the data obtained from the crystal of the mutant complex grown by the capillary counter-diffusion

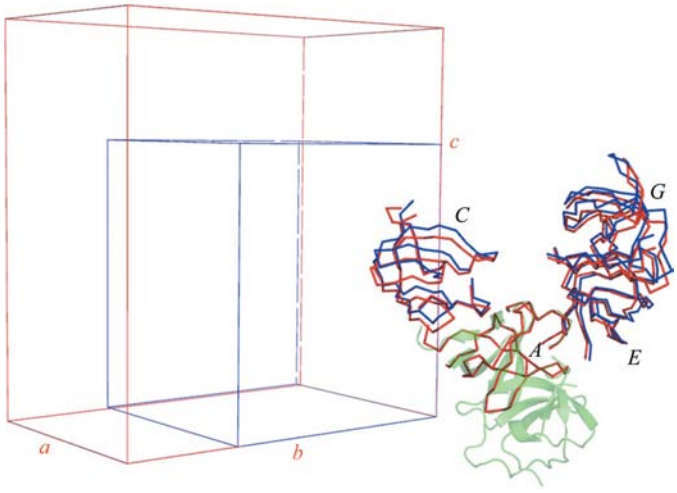

Figure 4
Comparison of the unit cell and packing of N114A Abl-SH3–p41 (green cartoon) and WT Abl-SH3–p41 (red ribbon) structures. The symmetry-related molecules of the mutant structure are shown as a blue ribbon superposed on the corresponding SH3 chains of the WT structure (chains *A*, *C*, *E* and *G*). The unit cells of the mutant (blue) and WT (red) crystals are shown.

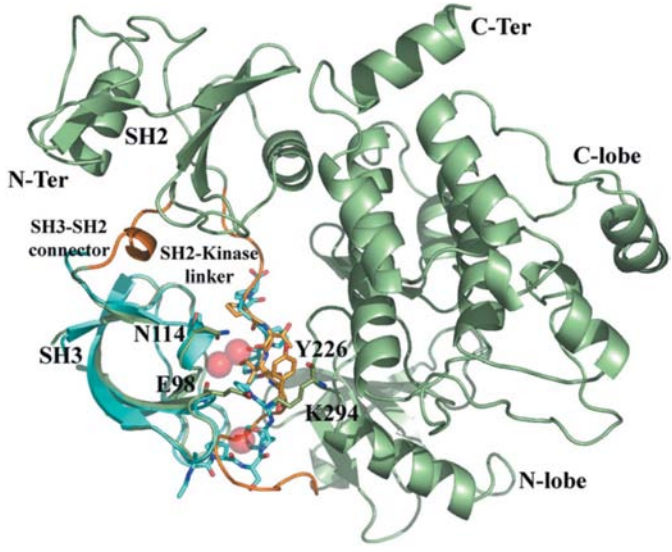

Figure 5
Superposition of the N114 Abl-SH3–p41 complex (cyan) and the Abl tyrosine kinase structure (PDB code 1opk; pale green). The SH2-kinase linker implicated in regulation of the kinase activity is coloured orange. Relevant water molecules are shown as red spheres.

technique allows accurate modelling of the solvent. Inspection of the binding interface of the complex between N114A Abl-SH3 and p41 reveals that most of the water molecules occluded at the binding interface in the WT complex are preserved in the mutant structure, with the exception of the more exposed water 2103, which is not found in the N114A complex. An equivalent situation is observed for the structure of the full-length Abl tyrosine kinase. Thermodynamic studies to determine the role of these buried water molecules are under way.

3.4. Comparison of the N114A Abl-SH3–p41 complex with the Abl tyrosine kinase structure

Many structures of SH3 domains and their complexes with peptide ligands have been solved to date, although in many instances the structure of the whole SH3-containing protein remains unsolved. In our case, the structure of the full-length Abl tyrosine kinase is available in active and autoinhibited assembled forms (Nagar *et al.*, 2003; Fig. 5). An important difference of the Abl tyrosine kinase in comparison with other tyrosine kinases is the substitution of the second proline in the SH2-kinase linker of the P*XX*P binding motif by tyrosine (Tyr226). The first proline residue, Pro223, binds to the first hydrophobic pocket formed by the Tyr115/Tyr70 residues of the SH3 domain. In the p41 complex, this pocket is occupied by Pro9 with very similar packing and distances. The second hydrophobic pocket, usually occupied by the second proline residue of the P*XX*P binding motif (Pro6 in the p41 complex), does not interact with any residues of the SH2-kinase linker. With regard to the specificity pocket, which is flanked by the RT loop, the SH2-kinase linker mostly interacts with Tyr70 at the beginning of the RT loop and Asn78. In the kinase structure this residue is involved in a hydrogen bond to Asn231 in the SH2-kinase linker, while in the mutant structure it forms a hydrogen bond to Gln103 from chain *B*. Asn78 lies next to the hydrophobic pocket formed by Trp110 and Trp99 in the SH3 domain, which is occupied by Pro2 of the p41 peptide in the SH3 complex and Pro230 in the kinase structure. An additional hydrogen bond that does not have a counterpart in the kinase structure is formed between Tyr4 of p41 and Asp77 in the RT loop (3 Å). It is interesting to note that the RT loop adopts different conformations in both structures, with a difference in the backbone position (r.m.s.d. > 2.5 Å).

In the autoinhibited tyrosine kinase structure, a salt bridge is established between Glu98 in the SH3 domain and Lys294 in the kinase domain (Fig. 5). Interestingly, Glu98 is placed in the n-Src loop, which shows the highest differences in the overall least-squares superposition of all the structures of the Abl-SH3 domain (WT and N114A mutant) solved at different pH values (Palencia *et al.*, in preparation). Moreover, the orientation of this residue changes as a consequence of the pH used in the crystallization of the N114A mutant and it is ligated to a buried water molecule that has been postulated to play an important role in the peptide-binding energetics (Palencia *et al.*, 2004). This water molecule (W4 chain *A*–*C* contact/W3 chain *B*–*D* contact) is conserved in the structure of the Abl-SH3–p41 complexes and also in the free forms of the WT and N114A structures. It is involved in hydrogen bonds to Ala114 (N, 3.01 Å), Ser113 (N, 3.29 Å), Glu98 (O, 2.9 Å) in the N114A Abl-SH3–p41 structure; the hydrogen-bonding distances are very similar in all reported structures. Interestingly, three additional water molecules (4, 9 and 66) buried upon binding of the p41 peptide are also present in the Abl tyrosine kinase structure (waters 35, 44 and 170). The presence of these water molecules in all the crystallographic structures of Abl-SH3 reported to date indicates that these conserved solvent molecules could also play a role in the autoinhibition of the Abl tyrosine kinase.

4. Conclusion

Crystals of the N114A mutant of the Abl-SH3 domain complexed with the high-affinity decapeptide p41 have been obtained by a modified capillary counter-diffusion technique. The technique allows the screening of the whole crystallization space with ammonium sulfate at six different pH values using less than 2 µl protein solution. The structure was solved from a complete data set collected at room temperature using crystals located inside the capillary in which they were grown, thus avoiding additional manipulation. The good quality of the crystals permits the accurate placement of the water molecules in the complex structures that have been postulated to play an important role in the peptide-binding energetics. A deeper understanding of the role played by the residues and solvent molecules located at the SH3 domain-binding site is the key to the rational design of new drugs effective for the treatment of diseases related to the malfunction of tyrosine kinases.

This work was funded by grants BIO2003-04274 and BIO2006-15517 from the Spanish Ministry of Science and Technology, grant 03-51-5569 INTAS from the European Union and grants from the Junta de Andalucía to the research teams FQM-171, RNM-143 and CVI-292, Project RMN-1344 and a research contract for JAG. We acknowledge the Spanish Ministry of Education and Sciences for the predoctoral research contract for AP and a Ramón y Cajal research contract for IL. This paper is a result of the Factoría de Cristalización funded by the program Consolider-Ingenio 2010.

References

Arold, S., O'Brien, R., Franken, P., Strub, M. P., Hoh, F., Dumas, C. & Ladbury, J. E. (1998). *Biochemistry*, **37**, 14683–14691.
Barila, D. & Superti-Furga, G. (1998). *Nature Genet.* **18**, 280–282.
Collaborative Computational Project, Number 4 (1994). *Acta Cryst.* D**50**, 760–763.
Emsley, P. & Cowtan, K. (2004). *Acta Cryst.* D**60**, 2126–2132.
García-Ruiz, J. M. (2003). *Methods Enzymol.* **368**, 130–154.
García-Ruiz, J. M. & González-Ramírez, L. A. (2006). Patent PCT/ES/2006/070004.

Laskowski, R. A., MacArthur, M. W., Moss, D. S. & Thornton, J. M. (1993). *J. Appl. Cryst.* **26**, 283–291.
Matthews, B. W. (1968). *J. Mol. Biol.* **33**, 491–497.
Musacchio, A., Saraste, M. & Wilmanns, M. (1994). *Nature Struct. Biol.* **1**, 546–551.
Nagar, B., Hantschel, O., Young, M. A., Scheffzek, K., Veach, D., Bornmann, W., Clarkson, B., Superti-Furga, G. & Kuriyan, J. (2003). *Cell*, **112**, 859–871.
Ng, J. D., Gavira, J. A. & García-Ruiz, J. M. (2003). *J. Struct. Biol.* **142**, 218–231.
Painter, J. & Merritt, E. A. (2006). *J. Appl. Cryst.* **39**, 109–111.
Palencia, A., Cobos, E. S., Mateo, P. L., Martinez, J. C. & Luque, I. (2004). *J. Mol. Biol.* **336**, 527–537.
Peranen, J., Rikkonen, M., Hyvonen, M. & Kaariainen, L. (1996). *Anal. Biochem.* **236**, 371–373.
Pisabarro, M. T., Serrano, L. & Wilmanns, M. (1998). *J. Mol. Biol.* **281**, 513–521.
Vagin, A. & Teplyakov, A. (1997). *J. Appl. Cryst.* **30**, 1022–1025.
Viguera, A. R., Arrondo, J. L, Musacchio, A., Saraste, M. & Serrano, L. (1994). *Biochemistry*, **33**, 10925–10933.
Winn, M. D., Murshudov, G. N. & Papiz, M. Z. (2003). *Methods Enzymol.* **374**, 300–321.